Optical Frequency Division & Pulse Synchronization Using a Photonic-Crystal Microcomb Injected Chip-Scale Mode-Locked Laser

Chinmay Shirpurkar, Jizhao Zang, Ricardo Bustos-Ramirez, *Member, IEEE*, David Carlson, Travis C. Briles, Lawrence R. Trask, Srinivas V. Pericherla, Di Huang, Ashish Bhardwaj, Gloria E. Hoefler, Scott B. Papp, and Peter J. Delfyett, *Fellow, IEEE*

(Top-Scored Paper)

***Abstract*—A mode-locked laser photonic integrated circuit with a repetition rate of 10 GHz is optically synchronized to a tantala-based photonic crystal resonator comb with a repetition rate of 200 GHz. The synchronization is achieved through regenerative harmonic injection locking using a coupled optoelectronic oscillator loop resulting in an optical frequency division factor of 20. The repetition rate of the photonic crystal resonator comb is stabilized and locked through electro-optic division. This stability is transferred to the mode-locked laser where we measure a fractional frequency instability of 8×10^{-11} at an averaging time of 10 s for the repetition rate signal of the mode-locked laser. Furthermore, we also measure the near carrier phase noise of the pulse repetition rate and estimate the integrated rms timing jitter of the pulses to be 6 ps.**

***Index Terms*—Photonic crystal resonator combs, photonic integrated circuits, semiconductor mode-locked lasers, electro-optic division.**

Manuscript received 17 February 2023; revised 24 May 2023; accepted 9 August 2023. Date of publication 14 August 2023; date of current version 16 February 2024. This work was supported in part by the DARPA DODOS Program under Grant HR0011-15-C-0057, in part by DARPA PIPES Program under Grant HR0011-19-2- 0016, and in part by the National Science Foundation under Grant IUCRC 2052701. *(Corresponding author: Chinmay Shirpurkar.)*

Chinmay Shirpurkar, Lawrence R. Trask, Srinivas V. Pericherla, Di Huang, and Peter J. Delfyett are with the CREOL, College of Optics and Photonics, University of Central Florida, Orlando, FL 32816 USA (e-mail: shirpurkar.chinmay@knights.ucf.edu; lawrencetrask@knights.ucf.edu; srinivasvarma@knights.ucf.edu; huangdileo@knights.ucf.edu; delfyett@creol.ucf.edu).

Jizhao Zang, Travis C. Briles, and Scott B. Papp are with the Time and Frequency Division, National Institute for Standards and Technology, Boulder, CO 80305 USA (e-mail: jizhao.zang@colorado.edu; travis.briles@nist.gov; scott.papp@nist.gov).

Ricardo Bustos-Ramirez is with the CREOL, College of Optics and Photonics, University of Central Florida, Orlando, FL 32816 USA, and also with the Infinera Corporation, Allentown, PA 18106 USA (e-mail: ricardo.bustos@knights.ucf.edu).

David Carlson is with the Time and Frequency Division, National Institute for Standards and Technology, Boulder, CO 80305 USA, and also with the Octave Photonics, Louisville, CO 80027 USA (e-mail: david.carlson@octavephotonics.com).

Ashish Bhardwaj and Gloria E. Hoefler are with the Infinera Corporation, Sunnyvale, CA 94089 USA (e-mail: abhardwaj@aurora.tech; ghoefler@infinera.com).

Color versions of one or more figures in this article are available at https://doi.org/10.1109/JLT.2023.3304605.

Digital Object Identifier 10.1109/JLT.2023.3304605

I. Introduction

OPTICAL frequency combs are a very powerful tool, being an integral part of applications such as optical frequency synthesis [1], high-speed \photonic digital signal processing [2] and high-speed optical interconnects [3], [4]. More recently, developments of compact chip-scale pulsed sources such as semiconductor mode-locked lasers [5] and microresonator based combs [6], [7] have shown tremendous promise in bringing experimental demonstrations out into real world systems. Therefore, the focus in the research community has been to push for compact energy-efficient combs capable of delivering comparable, or even better performance than bulky laboratory setups.

In order to have absolute knowledge of the position of each of the axial modes of an optical frequency comb it is necessary to know both the carrier-envelope offset frequency and its repetition rate frequency. Once these frequencies are determined accurately, we can generate a fully stabilized optical frequency comb. Determining the repetition rate of the comb, which is the rate at which pulses come out of the laser, is often straightforward and can be measured using a high-speed photodiode. The carrier-envelope offset which arises from the difference in phase velocity and group velocity of the pulses, requires self-referencing via f-to-2f interferometry [8] for accurate measurement. This in turn requires a coherent octave of optical bandwidth.

In this work we discuss two different types of integrated pulsed sources, namely the semiconductor mode-locked laser and the microresonator based frequency comb. Both these types of combs have their own advantages and disadvantages. We aim to select the best properties of both combs through optical synchronization. Semiconductor mode-locked lasers (MLL) have repetition rates ranging from 1 GHz to 10 s of GHz which can be easily detected using commercial high-speed photodiodes. They are easy to use, electrically pumped and extremely energy efficient. However, the output optical bandwidth is limited to 1-10 s of nm and several stages consisting of amplification, nonlinear broadening, and pulse compression are required to achieve a coherent octave of optical bandwidth. This can be challenging to achieve for semiconductor MLLs due to their

low pulse energies arising from GHz repetition rates and low output powers.

While mode-locked laser technology has been well known, precise dispersion engineering and developments in the fabrication of low-loss nonlinear waveguides have led to the development of compact high-Q microresonator-based comb sources. Traditionally, Kerr microresonators have been designed to have anomalous group-velocity dispersion (GVD) cavities which support various patterns and stationary states of the intracavity field including Turing patterns, modulational instability combs (MI), and dissipative Kerr solitons (DKS). DKS are low noise coherent comb states which have perfectly equidistant modes on the frequency grid. More recently, comb generation has also been achieved using normal GVD microresonator cavities by using unique resonator designs leading to interesting comb formation dynamics quite different than their anomalous GVD counterparts [9]. In this work we will be utilizing a normal GVD photonic crystal resonator design for comb generation. Further details regarding these photonic crystal resonators will be given in the next section.

Microresonator combs can produce pulses at repetition rates of 100 s of GHz or even 1 THz. These extremely high pulse repetition rates lead to extremely broad spectra which can make carrier-envelope offset stabilization possible [10]. However, the challenge with these combs are the >100 GHz repetition rates which cannot be directly measured with commercial integrated photodetectors. Therefore, we must rely on indirect methods to measure the repetition rates such as electro-optic division [11] or Vernier frequency division [12]. The more direct measurement methods require the use of uni-traveling carrier photodiodes [13] or frequency division using gain-switched semiconductor lasers [14]. In this work, we demonstrate a technique to obtain knowledge of the repetition rate frequency of a normal GVD 200 GHz photonic crystal resonator (PhCR) comb using optical frequency division down to 10 GHz. Using a technique known as regenerative harmonic injection locking [15] we can measure the repetition rate frequency of the PhCR and its frequency instability directly at the output of an InP-based semiconductor mode-locked laser photonic integrated circuit (MLL-PIC).

II. Fundamental Concepts, MLL-PIC & PhCR Comb

A. Regenerative Harmonic Injection Locking

The optical synchronization between the two independent pulsed sources discussed in this work relies on optical injection locking. The optical frequency division (OFD) using regenerative harmonic injection locking (RHIL) is an evolution of the coupled opto-electronic oscillator (COEO) multi-tone injection locking technique previously demonstrated for MLLs at different repetition rates [16]. The basic concept behind RHIL is as follows. We have a primary comb (in this case the PhCR comb) which has frequency tones ν_n defined as $\nu_n = \nu_{ceo} + n\nu_{rep}$, where ν_{ceo} and ν_{rep} are the carrier-envelope offset frequency and the repetition rate of the primary comb respectively. This primary comb is optically injected into a secondary comb (MLL-PIC) which has frequency tones f_m defined as $f_m = f_{ceo} + mf_{rep}$, where f_{ceo} and f_{rep} are the carrier-envelope offset frequency and the repetition rate of the secondary comb respectively. The mode numbers n and m are positive integer values. A basic schematic of the harmonic injection locking is shown in Fig. 1(a). Considering a single injected mode of the primary laser, if $\nu_{n_1} \approx f_{m_1}$ for some values of n_1 and m_1, the mode of the secondary laser f_{m_1} will synchronize in frequency and phase to the injected mode at ν_{n_1} provided the frequency difference between the two modes is within the injection locking bandwidth. Now if another set of modes n_2 and m_2 are also such that $\nu_{n_2} \approx f_{m_2}$, we will again have synchronization between modes f_{m_2} and ν_{n_2} (shown in Fig. 1(b)). The time domain representations of the optical pulses from both the primary and secondary combs are shown in Fig. 1(c). Since the secondary laser is an MLL, all axial modes will share a fixed phase relationship. Therefore, if two tones of the primary comb are simultaneously synchronized with the secondary comb, this effectively lines the repetition rate and carrier-envelope offset frequencies of the primary and secondary combs (shown in Fig. 1(d)).

$$\nu_{rep} = kf_{rep} \tag{1}$$

$$f_{ceo} = \nu_{ceo} + (n_2m_1 - n_1m_2)f_{rep} \tag{2}$$

This results in the relationships shown above, where $k = (m_1 - m_2)/(n_1 - n_2) = \Delta m/\Delta n$ and k is the optical frequency division factor. In this work, we only inject two adjacent tones of the PhCR comb which sets the condition $\Delta n = 1$ and therefore, k to be an integer value. In cases where ν_{rep}/f_{rep} is not an integer adjacent tones cannot be injected and (1) must be satisfied. In previous developmental work of this technique, the limitation of being unable to inject adjacent tones was resolved using the aid of electro-optic division [17]. However, in this case the primary comb is a perfect harmonic of the secondary comb and therefore the synchronization is more efficient and simplified. This technique has limitations for larger k values (such as $k > 10$) since the secondary comb (MLL-PIC) has to respond to frequencies much larger than it's natural repetition rate. To overcome these limitations, we also incorporate an intensity modulator (IM) to implement a COEO loop in the secondary comb. The COEO essentially serves as a pulse-picker which attenuates pulses from the primary comb that do not synchronize with the secondary comb while keeping synchronized pulses at maximum power (shown in Fig. 1(c)). It reduces phase slippage between the synchronized pulses and aids in long-term stability of the RHIL. It also increases the effective cavity Q of the secondary comb and reduces phase noise of the MLL.

We also implement electro-optic division (EOD) as an alternative technique to measure the repetition rate of the PhCR (ν_{rep}). This allows us to verify the accuracy of the repetition rate obtained through RHIL as both techniques should ideally provide the same measurements when done simultaneously. The EOD technique involves passing the light from the PhCR through a series of electro-optic phase modulators driven at a fixed frequency f_{eo}. The overlapping innermost axial modes will produce a residual beat signal f_{beat} which can then be used to measure the repetition rate of the PhCR accurately using the

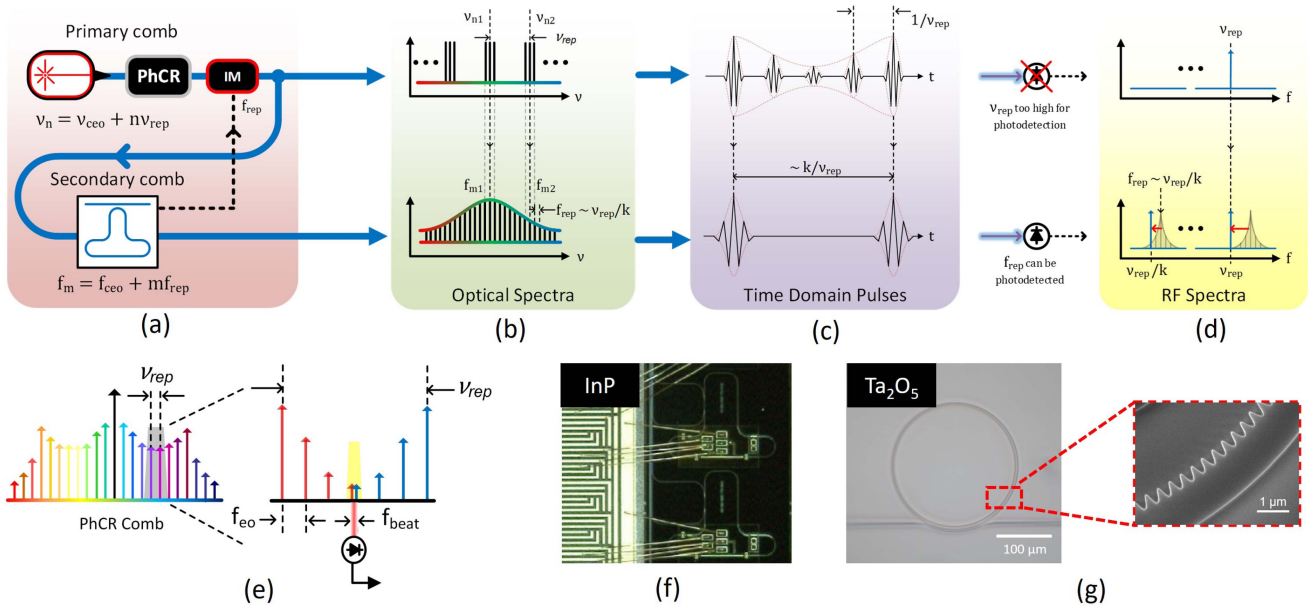

Fig. 1. (a) RHIL fundamental concept - a primary comb (PhCR, top) with a repetition rate of ν_{rep} is injected into a secondary comb (MLL-PIC, bottom) with a ν_{rep} that is a harmonic of the secondary comb repetition rate f_{rep}. A COEO loop is included for additional stability. (b) Optical spectral representation of the RHIL, the sidebands on the primary comb arise due to the COEO loop. (c) Optical pulses from both sources - COEO pulse picking aids in synchronization (d) RF domain representation of both sources - $f_{rep} = \nu_{rep}/k$ for a successful OFD. (e) Optical modes of PhCR with EO division showing a graphic representation of (3). (f) Micrograph of InP MLL-PIC. (g) SEM image of tantala PhCR ring with periodic modulation on inner waveguide wall highlighted.

relation,

$$\nu_{rep} = lf_{eo} + f_{beat} \tag{3}$$

A depiction of this method is shown in Fig. 1(e) where l is an integer (in this experiment $l = 6$). The f_{beat} signal can also be used lock the repetition rate of the PhCR by mixing it down with another stable oscillator to generate an error signal which acts as a feedback to the pump CW laser frequency. Locking the f_{beat} signal will eliminate repetition rate fluctuations of the PhCR caused by thermo-optic fluctuations in the resonator.

B. Mode-Locked Laser Photonic Integrated Circuit

In this experiment, the secondary comb used is an InP-based mode-locked laser photonic integrated circuit (MLL-PIC) in a racetrack configuration with a colliding-pulse architecture. The laser consists of a cavity with a free-spectral range (FSR) of ∼10 GHz, a gain section, a saturable absorber for passive mode-locking and a high-speed electro-absorption modulator (EAM). We utilize this EAM as a photodetector to measure the f_{rep} signal. The racetrack configuration also consists of multiple phase sections which can be used for wavelength and repetition rate tuning of the laser. A multi-mode interference coupler (MMI) with a split ratio of 85:15 provides the input for injection locking and the output port consists of an external semiconductor optical amplifier (SOA) to boost the power of the pulses. Further details on the laser layout and specifications can be found in [18]. A micrograph of the PIC is shown in Fig. 1(f).

C. Photonic Crystal Resonator

For our primary comb, we utilize a 200 GHz FSR tantalum pentoxide (Ta_2O_5 or tantala) based photonic crystal resonator (PhCR) designed with a normal GVD [9]. Although comb generation is conventionally not possible in normal dispersion resonators, the single mode defect of the PhCR enables phase matching for four-wave mixing. The PhCR rings have a periodic modulation on the inner waveguide wall that creates a photonic bandgap at one of the resonances, resulting as two split modes. The mode splitting is controllable through the amplitude of modulation of the inner waveguide wall [19]. This photonic bandgap leads to a localized region of high anomalous dispersion in an overall normal dispersion resonator. Pumping the lower frequency mode unconditionally satisfies the phase matching condition required for the initial degenerate four-wave mixing process. Further tuning of the pump laser to lower wavelengths can excite dark soliton pulses in the resonator. The unique design of the resonator reduces Turing patterns and chaotic states, allowing for comb generation even with arbitrarily slow frequency tuning of the pump laser. An SEM image of the resonator and the sinusoidal modulation is shown in Fig. 1(g). The dark pulse combs generated in the PhCR have the advantage of higher energy efficiency and better spectral flatness as compared to bright pulse combs. Comb states can be generated either in the forward or backward direction inside the ring and the underlying physics behind this is still being investigated [20]. In our experiments, we utilize the backwards generated comb since it usually provides much higher comb power than in the forward direction.

It is important to note the benefits that the tantala platform offers over conventional platforms such as silicon nitride. Tantala offers a slightly higher nonlinear index $n_2 = 6.2 \times 10^{-19}$ m^2/W, a smaller thermo-optic coefficient (8.8×10^{-6} 1/K) and a broader transparency window [21]. These factors along with tantala's high index of refraction and low temperature

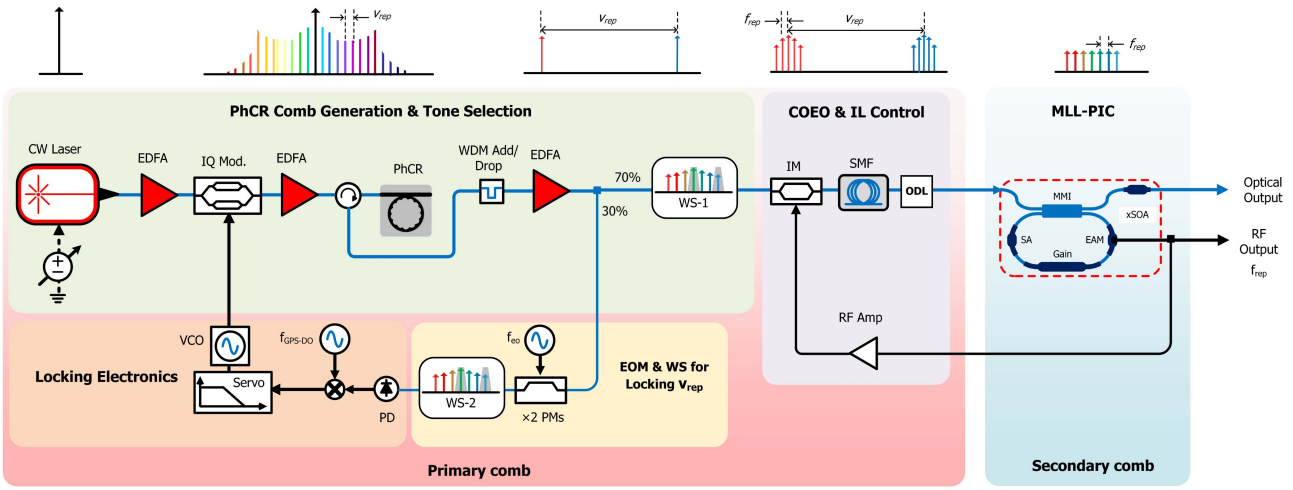

Fig. 2. Experimental setup for PhCR to MLL-PIC synchronization & OFD from 200 GHz to 10 GHz, WS-1: Waveshaper for RHIL, WS-2: Waveshaper for EOD, PM: Phase modulator, ODL: Optical delay line, VCO: voltage controlled oscillator, IM: Intensity modulator.

processing requirements make it an extremely attractive platform for nonlinear comb generation.

III. OFD Via RHIL - Experimental Setup

The experimental setup utilized is shown in Fig. 2. The PhCR comb is first generated by pumping the PhCR resonant mode with a tunable external-cavity diode laser having a linewidth of ∼100 kHz. The wavelength is controlled and detuned via external piezo modulation input into the laser to generate the comb. Slow piezo tuning is sufficient for comb generation as the PhCR avoids thermal relaxation dynamics associated with anomalous GVD resonators. We utilize the backwards comb which is collected through a circulator and the excessive pump power is suppressed using an add/drop WDM filter. The comb is amplified and split into two different paths. The first path goes into the electro-optic division (EOD) chain consisting of two phase modulators driven by a modulation frequency $f_{eo} \sim$ 33.37 GHz. The EO division chain generates overlapping tones near the midpoint of the adjacent comb lines as shown by (3) such that $l = 6$ and $f_{beat} \sim 10$ MHz. These two tones are isolated by a waveshaper (WS-2) for each pair of adjacent comb lines and photodetected. The f_{beat} signal generated is mixed down with a 10 MHz GPS disciplined oscillator (GPS-DO) to generate an error signal which is fed into a servo controller. The output of the servo goes to a voltage controlled oscillator (VCO) which drives an IQ modulator placed before the input to the PhCR. The IQ modulator is in a single-sideband suppressed-carrier (SSB-SC) configuration and is used to lock the repetition rate of the PhCR comb. Using the SSB-SC configuration for feedback to the pump wavelength offers greater locking bandwidth as compared to slow piezo tuning and compensates for pump frequency drifts, thermorefractive fluctuations and other environmental effects. The other path is input into another waveshaper (WS-1) which isolates the two comb lines to be injected into the MLL-PIC. The suppression provided by the waveshapers is >35 dB and does not pose any limitations to our experiment. We inject two adjacently spaced comb lines spaced by $\nu_{rep} \sim 200$ GHz into a MLL with a repetition rate $f_{rep} \sim 10$ GHz and demonstrate an optical frequency division factor of 20. These tones are then input into an electro-optic intensity modulator driven by the f_{rep} rate of the MLL-PIC before being injected. The f_{rep} signal used to drive the modulator is photodetected using the intracavity EAM of the MLL-PIC. This modulated light is delayed using ∼50 m of single-mode fiber (SMF) and passed through a tunable optical delay line (ODL) before being injected into the MLL-PIC. This completes the COEO loop and serves to increase the cavity Q of the MLL-PIC and also reduces phase noise of the f_{rep} signal. In the time domain, the COEO provides a sinusoidal modulation signal which provides low loss to one out of 20 pulses to improve overall stability and robustness. It is important to note that the SMF serves to increase the optoelectronic cavity Q of the COEO, whereas the tunable ODL serves to temporally align the pulses of the PhCR and MLL-PIC, while also ensuring that $f_{rep} \sim 10$ GHz is a subharmonic of $\nu_{rep} \sim 200$ GHz.

IV. Experimental Results

The optical spectrum of the PhCR comb is shown in Fig. 3(a) in a wide span and in Fig. 3(b) in a narrow span together with the optical spectrum of the MLL-PIC under passive mode-locking (PML). Fig. 3(c) shows the PhCR comb after EO division and the axial modes separated by ∼ 10 MHz which are to be isolated using a waveshaper (WS-2) and used to lock the repetition rate of the PhCR comb. An optical power of 40 μW is injected at the input port of the MLL-PIC but considering the split ratio of the MMI coupler, we have approximately 6 μW injected into the cavity (considering neglible facet/coupling losses at the input). The optical spectrum of the injected tones after the waveshaper WS-1 and COEO intensity modulator are shown in Fig. 4(a) along with the spectrum of the MLL-PIC before and after injection locking. It can be seen that RHIL results in distortion of the optical spectrum which is to be expected as the laser experiences greater gain around the wavelength region of the injected tones. The pulse intensity autocorrelation of the MLL-PIC pulses and the injected COEO modulated PhCR comb pulses are shown

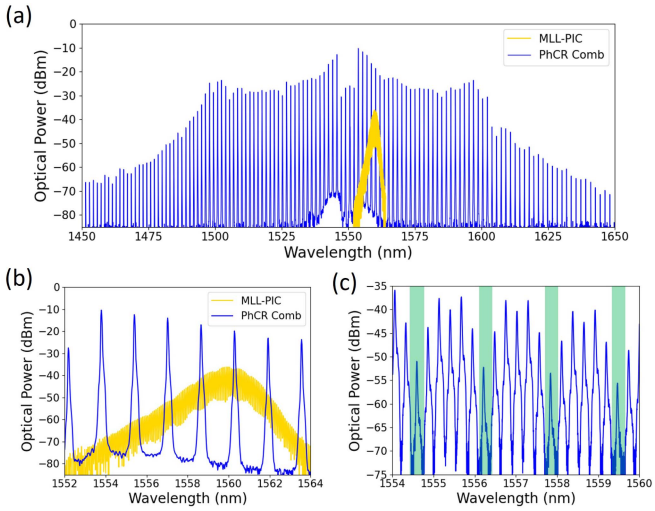

Fig. 3. Output optical spectrum of the PhCR comb (blue) and the MLL-PIC under PML (gold) on (a) a 200 nm span (b) on a 12 nm span. (c) EO divided PhCR comb - highlighted green tones are photodetected to get the $f_{beat} \sim$ 10 MHz signal.

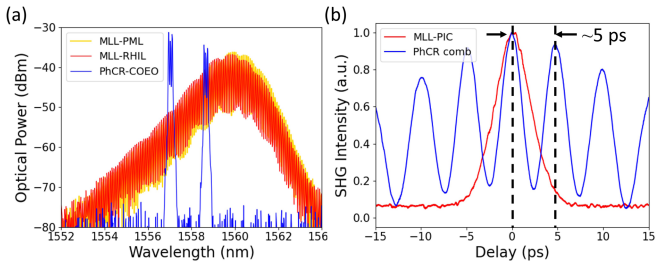

Fig. 4. (a) Optical spectrum of selected COEO modulated PhCR tones (blue), the MLL-PIC under PML (gold) and after RHIL (red) (b) Pulse intensity autocorrelation of PhCR comb (blue) and MLL-PIC (red).

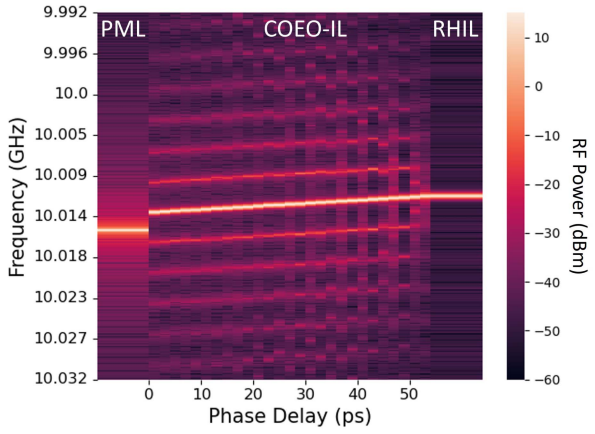

Fig. 5. f_{rep} signal of the MLL-PIC as the phase delay in the COEO loop is varied - the MLL goes from the PML regime to the COEO-IL regime to the RHIL regime.

in 4(b). The envelope on the intensity correlation trace of the PhCR pulse train results from the COEO modulation, and clearly shows how this modulation preferentially selects a pulse on the injection signal.

Fig. 5 shows the photodetected RF f_{rep} signal of the MLL-PIC in the three different regimes of operation as the phase delay

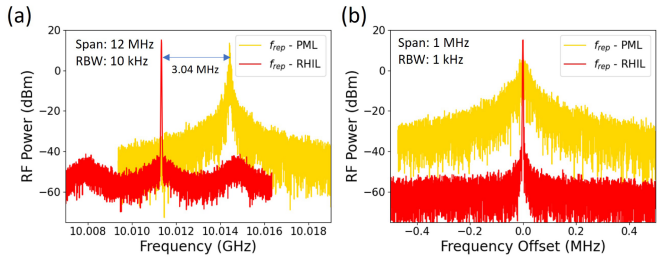

Fig. 6. RF spectrum of f_{rep} in PML (gold) and RHIL (red) states of the MLL-PIC (a) on a 12 MHz span (b) centered with respect to peak on a 1 MHz span.

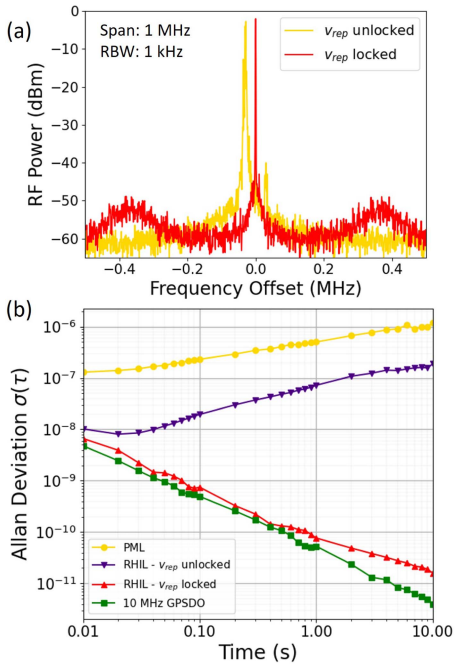

Fig. 7. (a) f_{beat} signal when ν_{rep} is locked and unlocked plotted relative to a 10 MHz center (b) Allan Deviation of MLL repetition rate under PML, RHIL with ν_{rep} unlocked, ν_{rep} locked, and the 10 MHz GPSDO signal used to lock ν_{rep}.

is tuned in the COEO loop. Initially, the laser is under the PML regime. As the delay is tuned, one set of modes (COEO modulated from a single mode ν_{n_1} of the PhCR comb) are injection locked to the laser leading rise to a COEO injection locked (COEO-IL) regime (starting at 0 ps in Fig. 5). As the delay is tuned further, the other set of modes (from the PhCR mode ν_{n_2}) are injected at which point OFD via RHIL occurs (at 54 ps in Fig. 5). This RHIL regime is where perfect synchronization between the two pulses occurs and a high-finesse photonic filter is created which suppresses the subsidiary tones from the COEO loop to create a single f_{rep} tone centered at the subharmonic of the PhCR comb repetition rate. After getting into the RHIL regime, we then lock f_{rep} of the PhCR.

The f_{beat} signal resulting from EO division before and after locking to the 10 MHz GPS-DO is shown in Fig. 7(a). The RF spectrum of the MLL-PIC under PML and after RHIL are shown in Fig. 6(a) over a 12 MHz span. A clear reduction of the phase noise sidebands is observed indicating a successful

RHIL. Fig. 6(b) shows the RF spectrum of the MLL-PIC before and after RHIL centered with respect to the peak frequency over a span of 1 MHz with 1 kHz resolution bandwidth (RBW) where both spectra are plotted relative to their peak frequencies. The repetition rate of the MLL-PIC after RHIL shifts from 10.014374 GHz to 10.011335 GHz resulting in a shift of 3.039 MHz. Experimentally, we have observed an injection locking bandwidth of approximately 10 MHz at the injection power of 40 μW. Using this data, we can compare the repetition rate measured via RHIL ($f_{rep-RHIL}$) to the one obtained using the EO division chain ($f_{rep-EOD}$). In the experiment, the modulation frequency is $f_{eo} = 33.369448938$ GHz. Since f_{beat} is locked to a 10 MHz GPS-DO and $l = 6$, we can use (3) to calculate the repetition rate of the PhCR comb to be $\nu_{rep} =$ 200.226693628 GHz.

Since our frequency division factor is 20, we can calculate $f_{rep-EOD} = 10.0113346814$ GHz from (1). Comparing this value to $f_{rep-RHIL} = 10.011335$ GHz, we get a difference of $\delta f = 0.3186$ kHz which is well within the 1 kHz resolution bandwidth of our measurements. It is important to note that the 10 MHz GPS-DO signal used to lock the repetition rate of the PhCR also acts as an external reference input to all RF instruments used throughout the experiment. These include RF synthesizers, RF spectrum analyzers and frequency counters. A common timebase reference for all instruments ensures accuracy and reliability in the measured data.

We measure the repetition rate frequency instability of the MLL-PIC to confirm that it inherits the instability limit imposed by the 10 MHz GPS-DO that locks the repetition rate frequency of the PhCR comb. The 10 GHz f_{rep} signal from the MLL-PIC is counted using a zero-dead time frequency counter. Using the frequency counter data, the Allan deviation is computed and plotted in Fig. 7(b). It is observed to follow a $1/\tau$ trend and matches closely with the measured allan deviation of the 10 MHz GPS-DO. The fractional frequency instability is measured to be 8×10^{-11} at an averaging time of 10 s which corresponds to a frequency instability of 800 mHz on a 10 GHz carrier.

We also measure phase noise of the f_{rep} signal using a carrier-noise test set to obtain a single sideband (SSB) phase noise spectrum. Since the photodetected repetition rate has a tendency to fluctuate due to environmental effects, we maintain source quadrature using an adjustable phase-locked loop (PLL). Normally, this invalidates data within the loop bandwidth, however the system carefully measures the PLL suppression curve and compensates for its effect. For the reference source, we use a RF synthesizer with a DCFM input which acts as the feedback for the PLL tuning voltage output of the carrier-noise test set. The RF synthesizer we use is a low frequency one, therefore in order to match the signal frequency to the reference source, we need to mix down the f_{rep} signal to a lower frequency. We mix down the ~10.012 GHz f_{rep} signal with a 10.24 GHz signal from an ultra low-noise sapphire loaded cavity oscillator (SLCO) to give a ~228 MHz signal. The phase noise of this mixed down 228 MHz signal is then measured relative to the RF synthesizer. The setup is depicted in Fig. 8(a). It is also important to measure the phase noise of the RF synthesizer we use as the reference in the measurements. In this measurement,

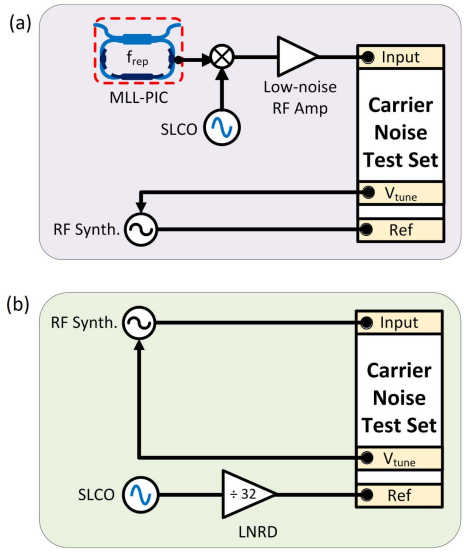

Fig. 8. (a) Setup for measuring phase noise of f_{rep} signal after RHIL. (b) Setup for measuring phase noise of RF synthesizer. LNRD: Low-noise regenerative divider, SLCO: Sapphire Loaded Cavity Oscillator.

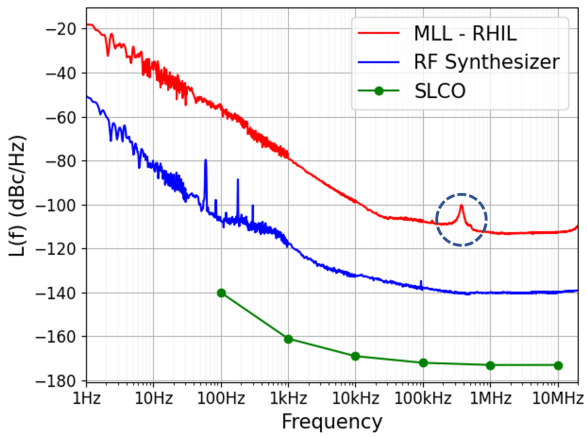

Fig. 9. Phase noise of mixed down MLL signal at 228 MHz relative to the RF synthesizer reference (red), phase noise of RF synthesizer reference at 320 MHz relative to ultra low-noise SLCO reference (blue) and absolute noise specifications of the SLCO reference are given (green). Circle at ~300 kHz in the MLL phase noise plot shows locking sidebands present on the PhCR injected modes due to the ν_{rep} lock.

the RF synthesizer output is the signal. For the reference we again use the ultra low-noise SLCO output of 10.24 GHz and divide it down to 320 MHz using a low-noise regenerative divider (LNRD). The phase noise of the synthesizer is then measured relative to the divided down 320 MHz signal of the SLCO using a PLL to maintain quadrature. This setup is depicted in Fig. 8(b). The compiled results of all measurements are plotted in Fig. 9 along with sample points of divided down SLCO phase noise at 320 MHz provided by the manufacturer. We can observe for f_{rep} (Fig. 9, red curve), the phase noise spectrum is limited by white frequency noise. The white phase noise floor above 1 MHz can be attributed to the thermal noise of the intracavity photodetector and the subsequent RF amplification stages. A small spike at ~300 kHz is also circled in the phase noise plot which is attributed to the locking sidebands present on the PhCR

injected modes due to the ν_{rep} lock. This can be verified by observing Fig. 7(a) where these locking sidebands can again be seen at ∼300 kHz on the locked f_{beat} signal. Assuming that the white phase noise floor at ~ -110 dBc/Hz extends out until the Nyquist frequency (5 GHz), we can estimate an rms timing jitter of 6 ps for our 10 GHz signal.

V. Conclusion & Outlook

In this work, we have presented a technique for direct optical frequency division of a photonic crystal resonator with a repetition rate of 200 GHz down to 10 GHz (division by 20) using regenerative harmonic injection locking with an MLL-PIC. We stabilize the repetition rate of the DKS and use both electro-optic division and RHIL to verify the accuracy of our technique. Our calculations show that the frequency division is accurate since the difference in our measurements is within the resolution bandwidth of our instruments. We measure a fractional frequency instability of the MLL-PIC to be 8×10^{-11} at an averaging time of 10 s. Finally, we also measure the phase noise of f_{rep} signal and estimate an rms timing jitter of 6 ps.

Experimentally, our technique has no limitations with regards to the absolute frequency values of f_{ceo}, ν_{ceo}, f_{rep}, and ν_{rep}. In particular as f_{ceo} is greatly tunable for the MLL, we can always align the primary comb mode to the second comb mode. However, there is a limitation that ν_{rep} has to be a close harmonic of the value of f_{rep} for the harmonic injection locking to occur. Additionally, the optical frequency division factor cannot be too large since the MLL may not be able to respond to injected tones with a frequency difference much larger than its gain bandwidth [15].

Future improvements of this technique will involve varying experimental parameters to further reduce phase noise and improving synchronization. Trends in RF stability & noise can be tracked as a greater number of tones (>2) are injected into the MLL-PIC. RF characteristics can be also studied by performing the experiment with CW pump lasers at different linewidths. The final goal would be for a fully integrated optical frequency divider. Hybrid integration of lasers with microresonator based combs via self-injection locking has already been demonstrated [22], greatly simplifying the comb generation process. Integrated wavelength filters can provide a more efficient method for selective tone injection compared to tabletop waveshapers. Integrating electro-optic modulators on a thin-film lithium niobate platform could also greatly compact the setup. Future steps towards integration could enable compact frequency comb applications in frequency metrology or optical atomic clocks.

Disclosures: David Carlson is a cofounder of Octave Photonics. The remaining authors do not currently have a financial interest in Ta_2O_5-integrated photonics.

References

[1] D. T. Spencer et al., "An optical-frequency synthesizer using integrated photonics," *Nature*, vol. 557, no. 7703, pp. 81–85, 2018.

[2] P. J. Delfyett et al., "Optical frequency combs from semiconductor lasers and applications in ultrawideband signal processing and communications," *J. Lightw. Technol.*, vol. 24, no. 7, pp. 2701–2719, Jul. 2006.

[3] K. Y. Yang et al., "Multi-dimensional data transmission using inverse-designed silicon photonics and microcombs," *Nature Commun.*, vol. 13, no. 1, 2022, Art. no. 7862.

[4] C. Shirpurkar et al., "Photonic crystal resonators for inverse-designed multi-dimensional optical interconnects," *Opt. Lett.*, vol. 47, no. 12, 2022, Art. no. 3063.

[5] P. J. Delfyett, I. Ozdur, N. Hoghooghi, M. Akbulut, J. Davila-Rodriguez, and S. Bhooplapur, "Advanced ultrafast technologies based on optical frequency combs," *IEEE J. Sel. Topics Quantum Electron.*, vol. 18, no. 1, pp. 258–274, Jan./Feb. 2012.

[6] T. J. Kippenberg, A. L. Gaeta, M. Lipson, and M. L. Gorodetsky, "Dissipative Kerr solitons in optical microresonators," *Science*, vol. 361, no. 6402, 2018, Art. no. eaan8083.

[7] T. C. Briles, S. P. Yu, T. E. Drake, J. R. Stone, and S. B. Papp, "Generating octave-bandwidth soliton frequency combs with compact low-power semiconductor lasers," *Phys. Rev. Appl.*, vol. 14, no. 1, 2020, Art. no. 014006.

[8] T. Udem, R. Holzwarth, M. Zimmermann, C. Gohle, and T. W. Hänsch, "Measuring the frequency of light with a mode-locked laser," *Opt. Commun.*, vol. 172, pp. 59–68, 1999.

[9] S. P. Yu, E. Lucas, J. Zang, and S. B. Papp, "A continuum of bright and dark-pulse states in a photonic-crystal resonator," *Nature Commun.*, vol. 13, no. 1, 2022, Art. no. 3134.

[10] T. E. Drake et al., "Terahertz-rate Kerr-microresonator optical clockwork," *Phys. Rev. X*, vol. 9, no. 3, 2019, Art. no. 31023.

[11] P. Del'haye, S. B. Papp, and S. A. Diddams, "Hybrid electro-optically modulated microcombs," *Phys. Rev. Lett.*, vol. 109, no. 26, pp. 1–5, 2012.

[12] B. Wang, Z. Yang, X. Zhang, and X. Yi, "Vernier frequency division with dual-microresonator solitons," *Nature Commun.*, vol. 11, no. 1, pp. 1–7, 2020.

[13] Q. Li et al., "High-power evanescently coupled waveguide MUTC photodiode with -GHz bandwidth," *J. Lightw. Technol.*, vol. 35, no. 21, pp. 4752–4757, Nov. 2017.

[14] W. Weng, A. Kaszubowska-Anandarajah, J. Liu, P. M. Anandarajah, and T. J. Kippenberg, "Frequency division using a soliton-injected semiconductor gain-switched frequency comb," *Sci. Adv.*, vol. 6, no. 39, 2020, Art. no. eaba2807.

[15] R. Bustos-Ramirez, L. R. Trask, A. Bhardwaj, G. E. Hoefler, F. A. Kish, and P. J. Delfyett, "Direct chip-scale optical frequency divider via regenerative harmonic injection locking," *Opt. Lett.*, vol. 46, no. 4, 2021, Art. no. 908.

[16] R. B. Ramirez et al., "Repetition rate stabilization and optical axial mode linewidth reduction of a chip-scale MLL using regenerative multitone injection locking," *J. Lightw. Technol.*, vol. 36, no. 14, pp. 2948–2954, Jul. 2018.

[17] R. Bustos-Ramirez et al., "Synchronization of electro-optically modulated Kerr soliton comb to a chip-scale mode-locked laser PIC via harmonic injection locking," *J. Lightw. Technol.*, vol. 40, no. 6, pp. 1742–1748, Mar. 2022.

[18] A. Bhardwaj et al., "A monolithically integrated racetrack colliding-pulse mode-locked laser with pulse-picking modulator," *IEEE J. Quantum Electron.*, vol. 56, no. 4, pp. 1–8, Aug. 2020.

[19] S. P. Yu, D. C. Cole, H. Jung, G. T. Moille, K. Srinivasan, and S. B. Papp, "Spontaneous pulse formation in edgeless photonic crystal resonators," *Nature Photon.*, vol. 15, no. 6, pp. 461–467, 2021.

[20] E. Lucas, S. P. Yu, J. Bush, and S. B. Papp, "Dark-pulse dynamics and directional switching in photonic-crystal ring resonators," in *Proc. IEEE Conf. Lasers Electro- Opt.*, 2021, pp. 1–2.

[21] H. Jung, S.-P. Yu, D. R. Carlson, T. E. Drake, T. C. Briles, and S. B. Papp, "Tantala Kerr nonlinear integrated photonics," *Optica*, vol. 8, no. 6, pp. 811–817, 2021.

[22] T. C. Briles et al., "Hybrid InP and SiN integration of an octave-spanning frequency comb," *APL Photon.*, vol. 6, no. 2, 2021, Art. no. 026102.